

Article

The Influence of Rate of Change in Confining and Pore Pressure on Values of the Modulus of Compressibility of the Rock Skeleton and Biot's Coefficient

Andrzej Nowakowski 

Laboratory of the Rock Deformations, Strata Mechanics Research Institute of the Polish Academy of Sciences, 30-059 Kraków, Poland; andrzej.nowakowski@imgpan.pl; Tel.: +48-508-996-905

Abstract: This work discusses the results of a study of the influence of rates of change of confining pressure on the result of a drained compressibility tests intended to determine the modulus of compressibility of a rock skeleton K_s . A series of cyclical compressibility tests was performed on samples of sandstone soaked in kerosene, for various rates of compression and decompression of the pressure liquid filling the cell and the pore volume of the sample. The studies showed that the deformability of the tested sample was directly proportional to the rate of change of the confining pressure. As a consequence, the value of the K_s modulus and Biot coefficient α decreased with increasing sample load rate. This phenomenon should be attributed primarily to equilibration of the liquid pressure inside the high-pressure cell with the liquid pressure in the sample pore space, caused by filtration of the pore liquid. These phenomena prove that the filtration process impacts the values of the modulus of compressibility of the rock skeleton K_s and of Biot coefficient α determined on the basis of the experiment. This is significant in the context of the use of Biot equations as constitutive equations for a porous rock medium.



Citation: Nowakowski, A. The Influence of Rate of Change in Confining and Pore Pressure on Values of the Modulus of Compressibility of the Rock Skeleton and Biot's Coefficient. *Energies* **2021**, *14*, 3056. <https://doi.org/10.3390/en14113056>

Academic Editor: Manoj Khandelwal

Received: 29 April 2021

Accepted: 19 May 2021

Published: 25 May 2021

Publisher's Note: MDPI stays neutral with regard to jurisdictional claims in published maps and institutional affiliations.



Copyright: © 2021 by the author. Licensee MDPI, Basel, Switzerland. This article is an open access article distributed under the terms and conditions of the Creative Commons Attribution (CC BY) license (<https://creativecommons.org/licenses/by/4.0/>).

Keywords: Biot medium; Biot coefficient; modulus of compressibility of rock; modulus of compressibility of rock skeleton; compressibility test; filtration

1. Introduction

The graph depicting consumption of gas as an energy source (Figure 1) based on information provided by [1] shows that during the period 2013–2019, natural gas was the source of 23.7% of delivered energy on average, where this value slowly increased from 2014, to reach 25.4% in 2019. These values clearly show the current importance of gas in the economy of the European Union. It should be noted that its share will probably increase in the near future, with the planned withdrawal of coal from use as an energy source (cf., e.g., [2]).

It should not thus be surprising that EU member states are dedicating much effort and money to seeking and exploiting their own deposits of natural gas. This requires them to extract gas from deposits located in extremely difficult geological conditions, or under dense urban areas with extensive industrial and communication infrastructure. The safe extraction of gas under such conditions is often a very significant technological and scientific challenge.

The facts cited above show that the extraction and storage of natural gas is still posing new and ever more complex problems, the solutions to which often require the employment of significant human and material resources. One of these problems is the correct determination of the mechanical properties of rocks forming the rock mass from which natural gas is extracted. A good example of such studies were the results of research on the properties of rocks from the Groningen gas deposit, published in [3,4].

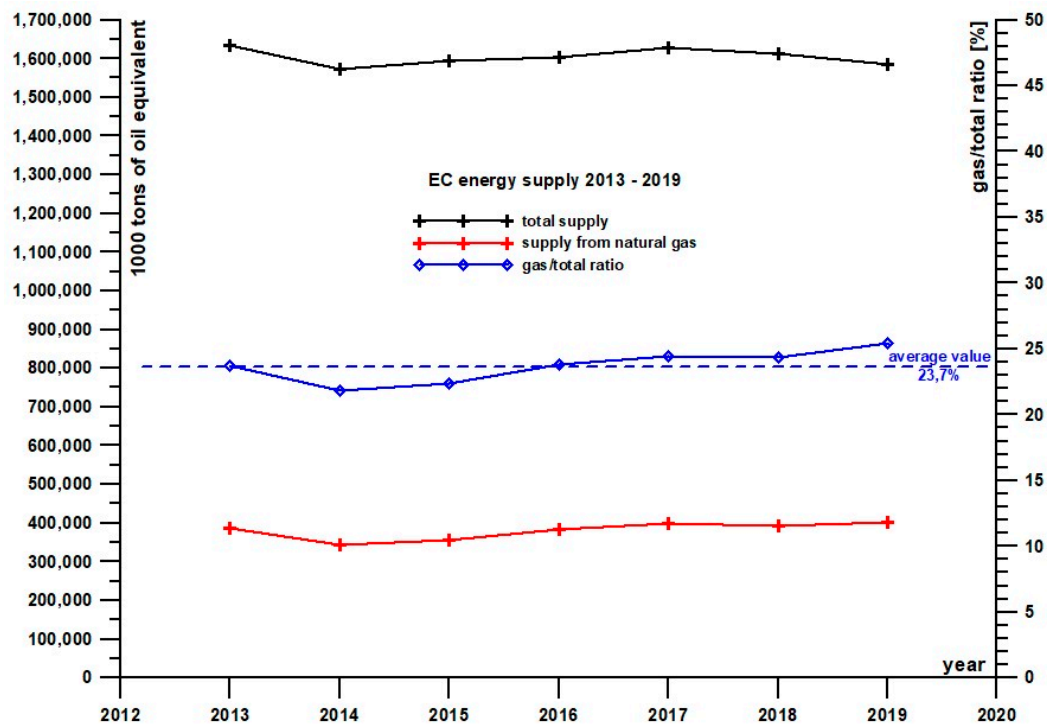


Figure 1. Energy obtained from natural gas compared with total energy obtained by the 28 European Union member states in 2013–2019 (in thousand tonnes of oil equivalent); according to EUROSTAT: 10 February 2021 [1].

In the case of a rock forming the gas deposit, such a determination requires the rock to be treated as a biphasic medium, composed of a solid phase (rock skeleton) and of pore space filled with fluid. The laboratory studies whose results are presented in this work served to establish how certain material constants of rocks (modulus of compressibility of the rock skeleton, Biot coefficient) vary as a function of the rate of change of pore fluid pressure. The results show that these constants decrease (most likely non-linearly) as the rate increases, a fact which—it would seem—should be taken into account when designing gas deposit exploitation strategies.

2. Material Identification—Constitutive Equation of the Medium

The main direction of research work on the course and effects of both extraction and underground deposition of gas should be identification of physical properties of the medium in which such processes occur. In practice, this means that a specific physical model should be assumed for the medium, for which relationships between stress and deformation are formulated, known as constitutive equations. In the case of soil or rock whose pore volume is filled with an inert pore fluid, the model of a porous elastic medium is a convenient physical model, the constitutive equations of which were derived by Maurice Anthony Biot on the basis of the equation for a uniform and isotropic elastic Hooke's medium. The work by Biot [5] provided for the first time a set of constitutive equations for a uniform, isotropic, and elastic porous medium, the pore volume of which is filled with a compressed, inert pore fluid, in the form:

$$\varepsilon_{ij} = \frac{(1 + \nu)}{E} \sigma_{ij} + \frac{\nu}{E} \sigma_{ii} \delta_{ij} - \frac{1}{3H} p_p \delta_{ij} \quad i, j = 1, 2, 3, \quad (1)$$

$$\zeta = \frac{\sigma_m}{H} - \frac{p_p}{R}, \quad (2)$$

here, the meanings of the symbols are as follows: σ_{ij} —the Cauchy stress tensor, ε_{ij} —the Cauchy deformation tensor, δ_{ij} —the so-called Kronecker's symbol, p_p —pore pressure, ζ —volume change of the pore space of the medium, E , ν —Hooke's elastic constants

(respectively, Young's modulus and Poisson's ratio), H , R —certain material constants introduced by Biot, σ_m —average stress, described by the formula:

$$\sigma_m = \frac{\sigma_{ii}}{3}. \quad (3)$$

The material constants H and R may be calculated using the following relationships:

$$\frac{1}{H} = \frac{1}{K} - \frac{1}{K_s}, \quad (4)$$

$$\frac{1}{R} = \frac{1}{K} - \frac{1+n}{K_s}, \quad (5)$$

where: K —volumetric elastic modulus of the medium, K_s —volumetric elastic modulus of the solid phase (skeleton) of the medium, n —porosity of the medium. On the other hand, the work [6] presented—by transforming Equation (1)—the so-called effective stress rule for a Biot medium in the following form:

$${}'\sigma_{ij} = \sigma_{ij} - \alpha p_p \delta_{ij} \quad i, j = 1, 2, 3, \quad (6)$$

where the coefficient α , given by the formula:

$$\alpha = 1 - \frac{K}{K_s}, \quad (7)$$

is known as Biot's coefficient. It should be noted here that the porosity of the studied material n is not explicitly present in Equation (7). We should remember that the values of volumetric compressibility moduli show a strong dependence on porosity, as was first pointed out in [7], and shown empirically e.g., in [8–10]. The form of Equations (4), (5), and (7) shows that correct determination of the values of volumetric compressibility moduli K and K_s is a *sine qua non* condition for practical application of both the effective pressure rule (6) and Biot Equations (1) and (2). The studies described in this work were carried out to determine a relationship between the value of the K_s modulus (and, as a consequence, of the α coefficient) and the rate of change of the confining pressure and the pore pressure.

The literature on Biot poroelastic medium is vast, in terms of both theoretical considerations and experimental studies. For example, the articles [11,12], expanded this theory—initially formulated for an isotropic medium—to the case of an anisotropic medium. This was also the direction taken, e.g., by the author of [13], who formulated the effective stress rule for a transversely isotropic material with structural anisotropy dictated by pore directions. Some synthetic works were produced by [14], who gave the results of applying the Biot equations to the case of specific elasticity theory problems, [15], who indicated the possibilities offered by Biot theory for describing phenomena occurring inside a rock treated as a biphasic porous medium, and [16], who analyzed the influence of pore pressure and of the scale effect on the form of the constitutive equations and the effective pressure rule for a Biot medium. This topic is certainly far from being exhausted from the theoretical point of view, as proven by the work [17], containing an interesting proof of the correctness of the effective stress theory formulated by Biot, and [18], showing extremely refined numerical modelling of a grainy, porous medium.

Authors of textbooks on rock mechanics have focused extensively (using different approaches) on the theory of a poroelastic medium. For instance, the book [19] (pp. 149–155) devoted a full chapter to poroelasticity based on analysis of the Biot medium equations, whereas in the [20] (pp. 168–204) the Biot's publications are mentioned only as literature supporting an extensive chapter on the equations for a poroelastic and thermoelastic medium. We should also mention the work [21], which includes a complete lecture on the poroelasticity theory, including the presentation of individual examples of practical applications of that theory.

The literature describing the results of laboratory studies on Biot media is at least as rich. The aforementioned publications [8–10] may be listed as examples (although certainly not exhaustive for the topic), these being core works aimed at giving a precise definition of terminology and research methodology. The following publications are similar in nature: [22], which includes a thorough analysis of the variability of Biot coefficient for various types of sandstone and limestone, and [23], which verified the method for determining Biot coefficient, previously proposed in [24]. Materials published by the American Rock Mechanics Association in 2013 include the work [25], related to phenomena occurring in rock during liquid saturation and pore pressure induction, as well as the paper [26] concerning the influence of the pore pressure on the value of Biot coefficient, and as a result, on the form of the effective pressure rule. On the other hand, paper [27] analyzed changes in permeability and in values of Biot coefficient taking place in high-porosity complex sandstones, with laboratory tests performed under conditions of constant mean stress or constant shearing stress.

The aforementioned examples naturally do not exhaust the topic, but they show that Biot consolidation theory remains a current tool, worthy of improvement, used in the analysis of processes occurring in an elastic, porous medium filled with a compressed pore fluid.

3. Determination of Values of the K and K_s Moduli—Compressibility Tests

Determining the parameter values for the equations for a Biot medium is not easy (cf., e.g., [28,29]), and experiments used to determine the volumetric elasticity moduli K and K_s are not trivial. These constants are determined on the basis of the results of a compressibility test, which involves compression of a rock sample using hydrostatic pressure, with simultaneous measurements of changes in the sample volume. It is assumed that this is a drained test, namely a test during which there is contact between the pore volume of the rock and the sample's environment. The compressibility test gives a relationship between the hydrostatic pressure p and the sample volume change e . The compressibility test is performed in two variants for the purpose of determination of the constants K and K_s :

(1) The $p_p = 0$ test

During this test, the sample is separated from the medium exerting hydrostatic pressure by means of an elastic shield, and the pore volume of the sample is in contact with air under atmospheric pressure. It may then be assumed that the deformation of the rock, including pores, does not result in changes to the pore pressure value p_p , which remains constant and equal to the atmospheric pressure. The results obtained by this means will henceforth be denoted by the label " $p_p = 0$ ".

(2) The $p_p = p$ test

During this experiment, the sample is placed in a high-pressure cell without shields, such that the pore volume of the sample is in contact with the liquid exerting hydrostatic pressure. The sample is previously saturated with the liquid, under vacuum.

Interpretation of the results of this test is based on the assumption that the pore pressure in the sample is continuously equal to the hydrostatic pressure. The importance of this assumption is underlined both by textbooks (e.g., [19,21]) and by authors publishing current results of studies on the properties of a poroelastic medium (e.g., [23]). If this is the case, it can be assumed that sample deformation is caused only by deformation of the rock skeleton, the pore volume of which is not deformed. The results obtained by this means will henceforth be denoted by the label " $p_p = p$ ".

Typical compressibility curves corresponding to the experiments discussed above are presented in Figure 2. Interpretation of the shape of these curves and of the characteristic points distinguished on the curves requires some prior remarks related to the rock structure.

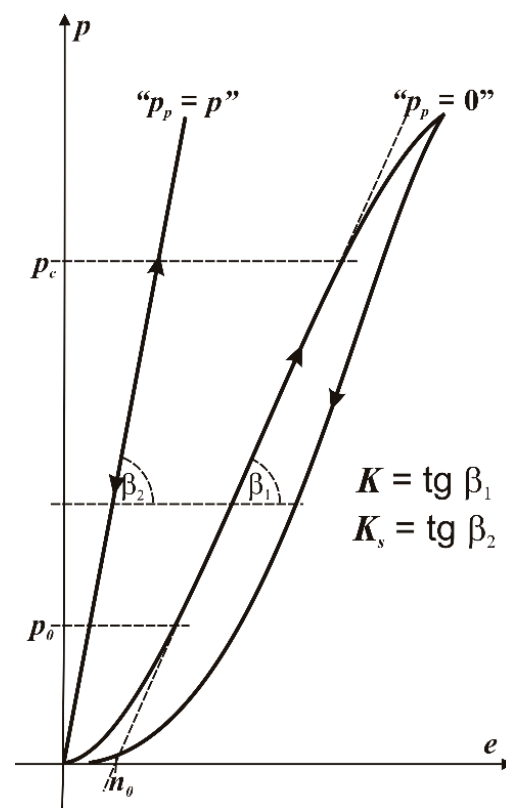


Figure 2. Typical compressibility curves (the arrows on the curves indicate the direction of pressure changes): K , K_s —compressibility moduli, p_0 , n_0 —crack closing pressure and crack porosity, respectively ([10]), p_c —pressure of rock consolidation; reproduced from [10], Arch. Min. Sci.: 1989.

It should be noted first that the so-called pore volume, comprised of void spaces of various shape and size, is an integral part of the rock. Based on their shape, the pores are divided into two groups: isometric pores, namely pores with all three dimensions similar and a more or less spherical shape; and cracks, namely pores of which one dimension is at least ten times smaller than the two other dimensions. In terms of the reaction of the rock to the hydrostatic pressure load, these two pore groups behave differently.

During the “ $p_p = 0$ ” experiment, isometric pores are generally not deformed under the influence of hydrostatic pressure, while above the wall resistance limit, the walls collapse, resulting in permanent destruction of the rock structure. On the other hand, cracks—because of their specific shape—“work”, that is, they may close or open, depending on the pressure exerted on the rock; this process is generally reversible and does not influence the rock structure, which is preserved.

The aforementioned differences in the behavior of isometric pores and cracks have significant influence on the shape of the “ $p_p = 0$ ” compressibility curve (see Figure 2). It should be noted that the initial part of this curve is non-linear, being convex towards the e axis. The non-linearity is a consequence of the process of crack closure under hydrostatic pressure. This process ends when the pressure p_0 , known as the crack closing pressure, is reached (cf. [12]), after which the compressibility curve becomes linear and remains linear up to the pressure value p_c , known as the consolidation pressure. The extension of the linear part of the “ $p_p = 0$ ” curve towards the e axis intersects that axis at a point with coordinates $(n_0, 0)$. The value of the abscissa for this point, n_0 , is the so-called crack porosity, which indicates what percentage of the volume of the tested sample consists of cracks. Once the hydrostatic pressure exceeds the value p_c , the “ $p_p = 0$ ” curve again becomes non-linear, being convex towards the p axis. This is caused by the beginning of destruction of the sample under the hydrostatic pressure.

The above statement is surprising in that if we assume that subjecting the rock to the hydrostatic pressure p results in hydrostatic stress inside the rock, this state should not destroy the material of which the sample is made. However, paper [30] proved that in a porous material, hydrostatic pressure may cause deviatoric stress conditions caused by crack surfaces sliding or by destruction of the walls of isometric pores. Relevant information on the influence of pores on the results of the compressibility test has been provided, e.g., in [9,10], while the authors of [18] used numerical modelling to illustrate processes occurring in a grainy, porous medium and their influence on the values of the material constants of a Biot medium.

It should also be noted that most rocks have a grainy structure, and grain contact points may be extremely strong stress concentrators, which means that point stresses several orders of magnitude stronger than the load pressure may occur in a rock subjected to hydrostatic pressure. Stress concentrators may also include crack edges, from which material destruction very often begins. The result may be a superposition of several processes, which—once the consolidation pressure is exceeded—may destroy the rock structure.

The situation is different in the case of the “ $p_p = p$ ” test. If the pore fluid pressure is equal to the hydrostatic pressure, pore shape and volume do not change, and changes of sample volume, if any, are a result only of the compressibility of the rock matter (with accuracy limited to the compressibility of the pore fluid). As a result, the “ $p_p = p$ ” compressibility curve is linear as a rule within the entire range of hydrostatic pressures. A deviation from this rule occurs only when isolated cracks, namely cracks into which the pore pressure cannot penetrate, account for a significant share of all cracks in the tested material. The initial part of the “ $p_p = p$ ” curve then becomes convex towards the e axis, as a consequence of the closing of such cracks. An example is shown in Figure 3.

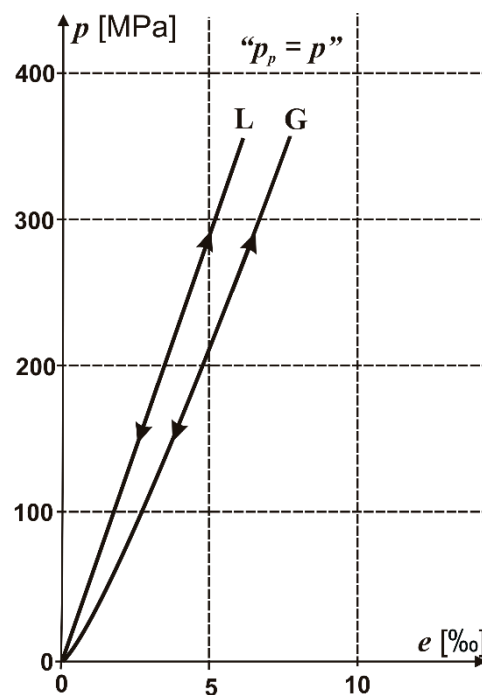


Figure 3. Compressibility curves “ $p_p = p$ ”: L—material without isolated cracks (limestone from stone pit Morawica), G—material with isolated cracks (granite from stone pit Strzelin); reproduced from [10], Arch. Min. Sci.: 1989.

The sought moduli of compressibility of the rock (K) and of its skeleton (K_s) are the tangents of the angles β_1 and β_2 , shown in Figure 2. These are the angles of inclination of the linear parts of the curves, respectively, $p_p = 0$ and $p_p = p$, to the horizontal axis, as shown in Figure 2 (for details see [31]). It is clear that the condition $K_s \geq K$ holds, with $K_s = K$ when the rock porosity satisfies the condition $n = 0$.

4. Testing and Measurement Equipment

The compressibility tests whose results are discussed here were performed using a GTA-10 device located at the Rock Deformation Laboratory, Strata Mechanics Research Institute, PAS in Kraków, Poland. This device includes a Kármán type cell enabling conventional, triaxial compression tests to be performed according to the methodology described by [32], a set of hydraulic amplifiers of hydrostatic and pore pressure, and a high-pressure pump supplying the piston and hydraulic amplifier system. The maximum hydrostatic pressure achieved inside the cell and the maximum pore fluid pressure are equal, and have the value 400 MPa. The maximum load force generated by the piston is 1500 kN. A diagram of the GTA-10 device is presented in Figure 4, and detailed information on its use is given by [33,34].

GTA-10 triaxial testing system

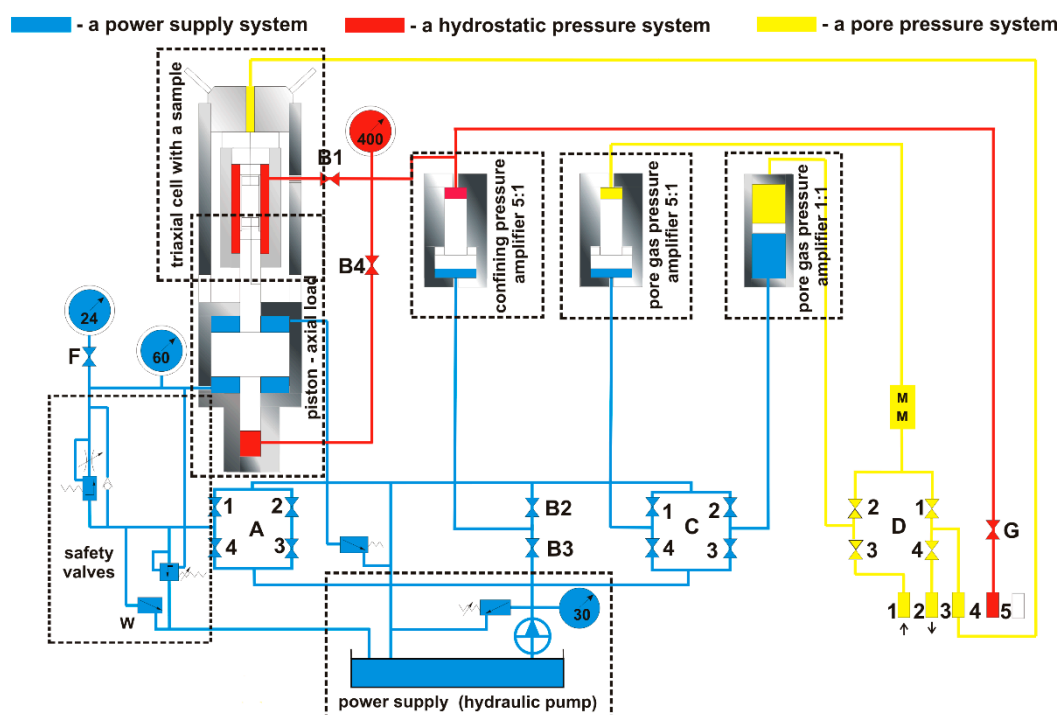


Figure 4. Diagram of the GTA-10 device: A1, A2, A3, A4—valves controlling the movement of the press piston, B1, B4—valves that control the flow of liquid in the high pressure cell, B2, B3—valves controlling liquid pressure in a triaxial cell through a pressure amplifier with a ratio of 5:1, C1, C2, C3, C4—valves controlling pore pressure in a sample through a low pressure amplifier with a ratio of 1:1 (on the right) and high pressure amplifier with a ratio 5:1 (on the left), D1, D2, D3, D4—valves controlling the flow of pore gas to and from inside the tested sample; reproduced from [31], Arch. Min. Sci.: 2021. Reproduced from [31], Polish Academy of Sciences, Committee of Mining: 2021.

Linear deformation of a sample was measured using a core-free inductive sensor attached to bands placed on the sample edge (for details see [35]). A sensor, in the form of a single-layer, core-free coil (Figure 5), is connected to an oscillating LC circuit via pressure electric glands in the plug of the high-pressure cell. Deformation of the sample changes the inductance of the sensor, and thus the oscillation frequency of the LC circuit. Frequency changes, which can be easily measured, are recorded and converted to sample deformation values. As very large pressure differences are present inside the cell, and the accompanying temperature changes can be as high as 50 C, a reference sensor made identical to the measuring sensor, installed on a steel support and placed inside the pressure cell, was used to correct the indications of the measurement sensor. Both sensors are alternatively connected to the same generator via a transistor-type switch, thus reducing the influence

of changes in the power supply voltage and the ambient temperature on the generator. The volumetric deformation of the sample e was calculated on the basis of measured linear deformation, assuming uniformity and isotropy of the sandstone material.

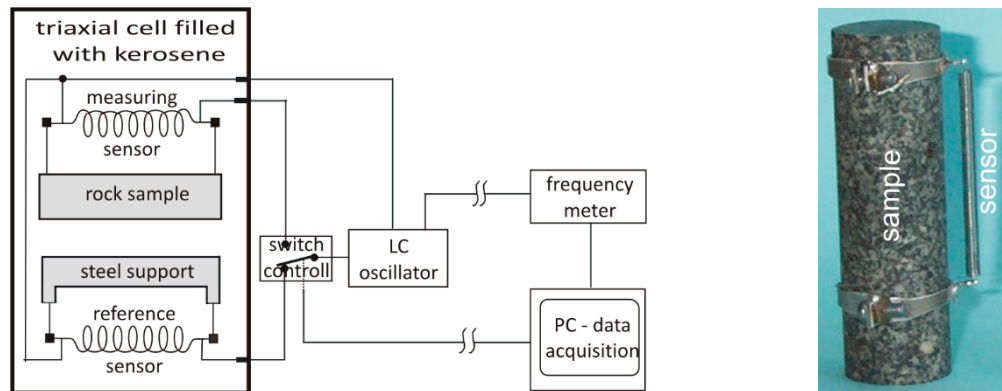


Figure 5. The idea behind the measurement of deformation using an inductive sensor in a reference system (**left**) and a photograph of a sensor installed on a sample (**right**); reproduced from [35] Int. J. Rock Mech. Min. Sci. Geomech. Abstr.: 2004. Reproduced from [35], the name of the publisher Elsevier: 2004.

5. Test Subject

The subject of the test was a cylindrical sample made of sandstone obtained from a rock quarry located in Tumlin (this will henceforth be referred to as Tumlin sandstone). It is a sedimentary rock with compact and disordered texture. The structure is of medium psammite type. The skeleton is grainy and compact, well sorted. The grain diameter usually lies in a range from 0.1 to 0.3 mm; finer grains (0.05–0.1 mm) are less common. The grains are usually weakly coated.

The grain skeleton includes mainly quartz grains (over 90% of grains). This is usually monocrystalline quartz, with normal or slightly undulose extinction. Polycrystalline grains are found very rarely. The composition of the skeleton further includes a small number of silicate rock grains made of chalcedony and single potassium feldspars (orthoclase), kaolinite aggregates and strongly weathered muscovite platelets.

The binder is of a contact-pore type, quartz-iron, accounting for up to 15% of the rock volume. Regenerative quartz binder is dominant and fills the pore volume almost entirely. The original shape of regenerated quartz grains is underlined by thin (several micrometers thick) rims made of weakly translucent, brownish, cryptocrystalline iron oxides and hydroxides. Only ferrous-loamy binder made of microcrystalline iron hydroxides and very fine platelets or fibers of clay minerals—mainly illite, more rarely hydromuscovite—are observed in areas with tighter grain packing. Larger pores are usually filled with microquartz. A more complete petrographic description of the Tumlin sandstone is provided in [36].

Pycnometric studies have shown that the volumetric density (ρ) of Tumlin sandstone is approximately 2.43 g/cm^3 with a porosity (n) not exceeding 8%. Uniaxial compression tests have shown that the compressive strength of this sandstone is in the order of 90 MPa, its Young's modulus is in the order of 24 MPa and the Poisson's ratio is in the order of 0.20.

6. Scope of Testing and Methodology

The testing program and methodology were developed to verify the statement that during the " $p_p = p$ " compressibility test, the pore pressure in the sample p_p is always equal to the hydrostatic pressure inside the pressure cell, i.e., the confining pressure p . This statement was deemed dubious because, assuming a constant volume of the high-pressure cell, equilibration of confining pressure and pore pressure may take place mainly through transport of fluid mass from the environment of the sample to or from its pore volume, namely by fluid filtration. The rate of filtration depends on many factors and is certainly

finite. It should thus be suspected that changes in the pore pressure occur with some delay with respect to changes in the confining pressure. Moreover, it may be supposed that this delay will be greater when the confining pressure changes at a higher rate.

A drained compressibility test in the “ $p_p = p$ ” version was used to verify these hypotheses. The assumption was made that the material is not destroyed during such a test, and thus this test may be performed multiple times using the same sample. A range of experiments was performed, in which the compressibility of a Tumlin sandstone sample was studied for various rates of compression and decompression of the liquid filling the pressure cell in which the sample was submerged. The applied rates of change of confining pressure were determined by the technical capacity of the GTA-10 device and were as follows: minimum rate 0.5 MPa/s, maximum rate 8.0 MPa/s. The maximum hydrostatic pressure was 360 MPa. The following experiment types were planned:

(A) “slow loading—various unloading” (SL).

Five “loading—unloading” loops were performed, such that the rate of increase of the confining pressure (henceforth referred to as loading rate or compression rate) was constant in each of the loops and equal to 0.5 MPa/s, while the rate of decrease of the confining pressure (henceforth referred to as unloading rate or decompression rate) had the following values: 0.5 MPa/s, 1.0 MPa/s, 2.0 MPa/s, 4.0 MPa/s, and 8.0 MPa/s.

(B) “fast loading—various unloading” (FL).

Five “loading—unloading” loops were performed such that the loading rate was constant in each of the loops and had the value 8.0 MPa/s, while the unloading rate had the following values: 0.5 MPa/s, 1.0 MPa/s, 2.0 MPa/s, 4.0 MPa/s, and 8.0 MPa/s.

(C) “various loading—slow unloading” (SU).

Five “loading—unloading” loops were performed such that the loading rate had the following values: 0.5 MPa/s, 1.0 MPa/s, 2.0 MPa/s, 4.0 MPa/s, and 8.0 MPa/s, while the unloading rate was constant in each of the loops and had the value 0.5 MPa/s.

(D) “various loading—fast unloading” (FU).

Five “loading—unloading” loops were performed such that the loading rate had the following values: 0.5 MPa/s, 1.0 MPa/s, 2.0 MPa/s, 4.0 MPa/s, and 8.0 MPa/s, while the unloading rate was constant in each of the loops and was equal to 8.0 MPa/s.

The values of loading and unloading rates for the experiments described under (A), (B), (C), and (D) are summarized below (Table 1).

Table 1. Loading and unloading rates for cyclical experiments described under (A), (B), (C), and (D).

Test Type	Loop Number	Loading Rate	Unloading Rate	Test Type	Loop Number	Loading Rate	Unloading Rate	
SL	1	0.5 MPa/s	0.5 MPa/s	SU	1	0.5 MPa/s	0.5 MPa/s	
	2		1.0 MPa/s		2			1.0 MPa/s
	3		2.0 MPa/s		3			2.0 MPa/s
	4		4.0 MPa/s		4			4.0 MPa/s
	5		8.0 MPa/s		5			8.0 MPa/s
FL	1	8.0 MPa/s	0.5 MPa/s	FU	1	8.0 MPa/s	8.0 MPa/s	
	2		1.0 MPa/s		2			1.0 MPa/s
	3		2.0 MPa/s		3			2.0 MPa/s
	4		4.0 MPa/s		4			4.0 MPa/s
	5		8.0 MPa/s		5			8.0 MPa/s

In these experiments, in thermodynamic terms, the liquid filling the high-pressure cell underwent an isochoric transformation. This means that the liquid temperature varied during both loading (compression) and unloading (decompression) of the sample, where the amplitude of the changes reached even 50 C. For this reason, loading and unloading

did not follow each other immediately, but were separated by a temperature stabilization phase, the duration of which depended on the compression or decompression rate. The temperature was considered stable after compression when the difference between the initial and the final temperature was not greater than 3 C, and after decompression when the difference did not exceed 0.5 C. This assumption was adopted because the liquid temperature drop inside the cell after compression was slower than its increase after decompression. The temperature of the liquid inside the pressure cell was measured using the p - n connector of a green LED diode (see [37]).

Kerosene was used as the pore fluid in the described experiments. It was assumed that kerosene can be considered as an inert liquid and its viscosity is low enough for easy penetration into the pore space of the rock. The author was aware that water was the most common pore liquid in nature. The problem, however, was that—according to the author—water could not be considered as an inert fluid.

7. Results

For a sample made of the material described in chapter 5, the experiments described under (A)–(D) in chapter 6 were performed. All of these experiments were performed using the same sample. In the analysis of the results, it was assumed—on the basis of previous studies ([31])—that the value of the modulus of volumetric compressibility of the studied rock is

$$K = 21.5 \text{ GPa}, \quad (8)$$

The results obtained are discussed below, beginning with the tests in which the loading rate was identical in each loop, while the unloading rates were different.

(A) The “slow loading—various unloading” (SL) test.

The result of the SL test is shown in Figure 6. The figure shows the relationships between the hydrostatic pressure p and the temperature in the cell t (on the left), and between the hydrostatic pressure p and the sample volume change e (on the right).

The $p(t)$ curves in Figure 6 show that the temperature changes during compression are identical in each case, both qualitatively and quantitatively. The volume change $p(e)$ is also repeatable during compression. Thus, in Figure 6, only one compression line is given for the $p(e)$ curves, labelled “compression— 0.5 MPa/s^{-1} ”, and this was taken as representative for all such lines.

In the case of decompression, the $p(t)$ curve (Figure 6, left) begins with a small pressure drop Δp , caused by a temperature drop at the end of compression. The corresponding section of the $p(e)$ curve (Figure 6, right) is not distinguished in any way. As all decompression lines on the $p(e)$ curves virtually overlap, the changes of sample volume during unloading may be considered independent of the decompression rate and the large temperature changes accompanying the unloading. It can even be said that at low compression rates, the decompression rate is insignificant for the mode of deformation of the sample. If we denote the modulus of compressibility of the skeleton of the tested sample by $K_{s(c)}$ for loading (compression) and $K_{s(d)}$ for unloading (decompression), then on the basis of the relationships shown in Figure 6, it may be assumed that the following holds for the SL test:

$$K_{s(c)} = K_{s(d)} = 32.6 \text{ GPa}. \quad (9)$$

Using the values of (8) and (9) in the Formula (7), we obtain a value of Biot’s coefficient for the “slow loading—various unloading” test equal to:

$$\alpha = 1 - \frac{21.5}{32.6} \approx 0.34. \quad (10)$$

(B) The “fast loading—various unloading” test (FL)

The respective relationships for this test are shown in Figure 7. Additionally, in the case of this test, the change of sample volume during loading was identical for all loops,

and thus a single compression line, labelled “compression—8.0 MPa/s”, is presented as the representative line. It was thus concluded that:

$$K_{s(c)} = 34.8 \text{ GPa.} \quad (11)$$

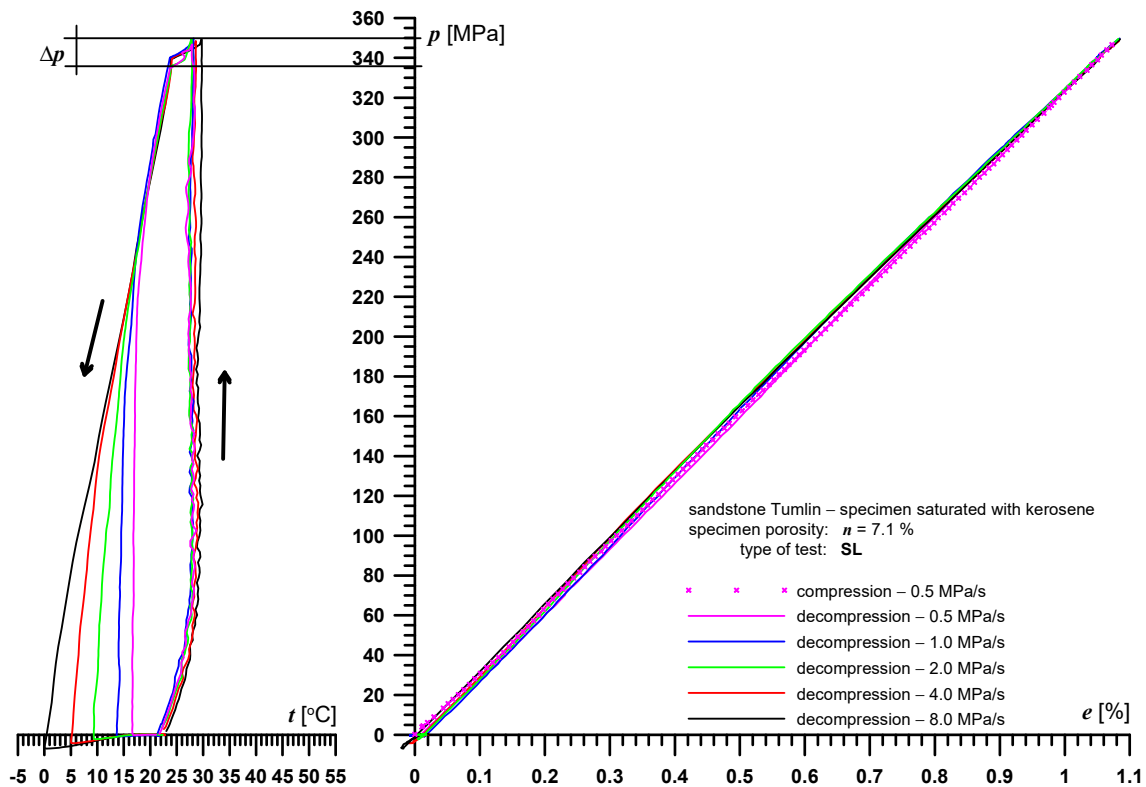


Figure 6. SL test result for Tumlin sandstone. **Left:** relationship between hydrostatic pressure and temperature (the arrows indicate the direction of change of hydrostatic pressure), **right:** relationship between hydrostatic pressure and volume change.

In the FL test, the temperature after compression was much higher than in the SL test, and, as a consequence, the pressure drop Δp accompanying the temperature drop was greater as a result of heat release into the environment (Figure 7, right). The shape of the $p(t)$ curves in Figure 7 may be considered to be qualitatively identical to that in Figure 6.

Analysis of the shape of the decompression curves $p(e)$ (Figure 7, right) shows that the decompression lines for the sample in the FL test virtually overlap and are significantly different from the compression lines. It was thus concluded that the following can be assumed for all decompression curves in this test:

$$K_{s(d)} = 41.2 \text{ GPa.} \quad (12)$$

This means, however, that in the case of compression and decompression we have different values of Biot’s coefficient, denoted respectively as $\alpha_{(c)}$ and $\alpha_{(d)}$. These values are as follows:

$$\begin{aligned} \alpha_{(c)} &= 1 - \frac{K}{K_{s(c)}} = 1 - \frac{21.5}{34.8} \approx 0.38 \\ \alpha_{(d)} &= 1 - \frac{K}{K_{s(d)}} = 1 - \frac{21.5}{41.2} \approx 0.48 \end{aligned} \quad (13)$$

The difference in the slope of the compression and decompression lines relative to the horizontal axis (Figure 7) is a consequence of the change in the volumetric deformations of the sample Δe , occurring during temperature stabilization inside the cell, taking the form of swelling. A question arises as to the cause of this phenomenon.

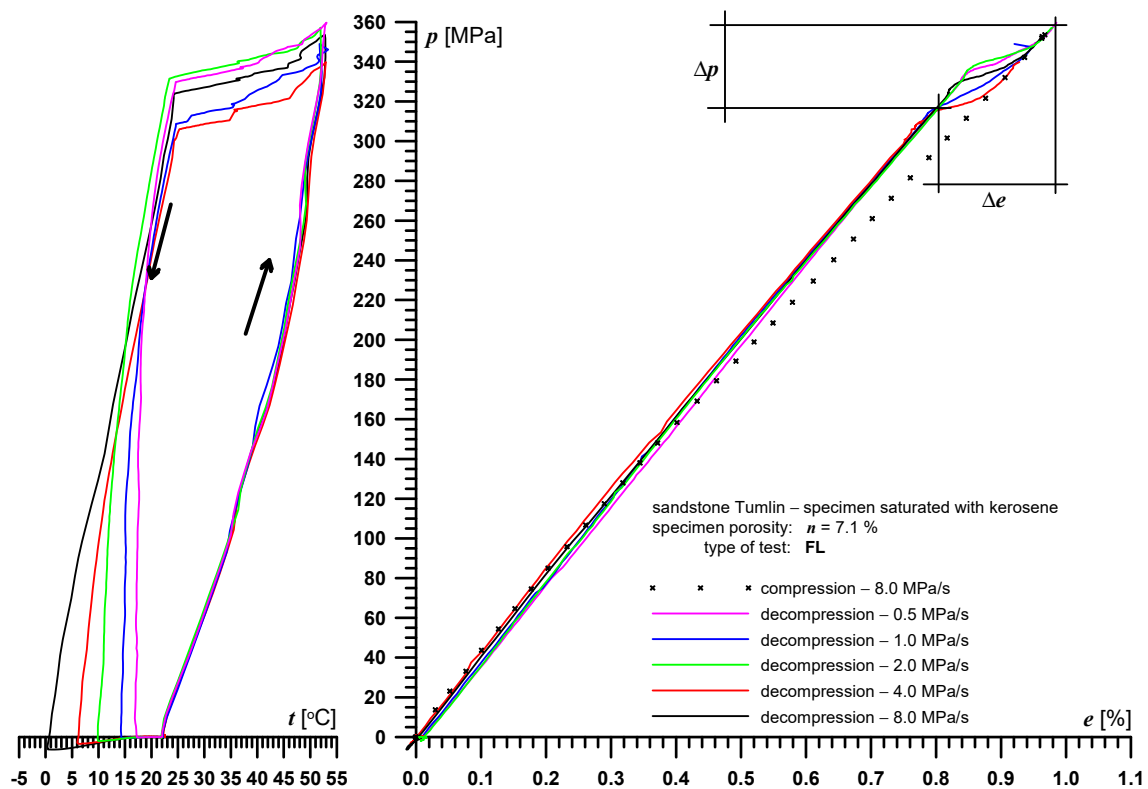


Figure 7. FL test result for Tumlin sandstone. **Left:** relationship between hydrostatic pressure and temperature (the arrows indicate the direction of change of hydrostatic pressure), **right:** relationship between hydrostatic pressure and volume change.

It would seem that in this case the swelling (Δe) is a consequence of two effects: the aforementioned drop in the confining pressure as a result of liquid temperature drop inside the cell, and fluid filtration into the pore volume of the rock during the equilibration of the confining and pore pressures. The high rate of increase in confining pressure resulted not only in a significant increase in liquid temperature inside the cell, but also in a delayed response of the pore pressure to the confining pressure. Only when the confining pressure stopped increasing (at the end of compression) did filtration lead to an equilibrium between the pressures inside and outside the sample.

This hypothesis was confirmed by comparison of the values of the modulus of compressibility of the rock skeleton obtained in this test for sample compression and decompression. The modulus for compression was calculated as $K_{s(c)} = 34.8$ GPa, and the modulus for decompression as $K_{s(d)} = 41.2$ GPa, a difference of approximately 20%. The equilibration of pressure causes the volumetric deformations of the sample to decrease, and its volumetric modulus of elasticity increases.

In the experiments discussed above, the sample was loaded at an identical rate in all cases, while the unloading rates were different. For the following two cyclical tests the situation was reversed: the sample was loaded at various rates, while the unloading rate was constant.

(C) “Various loading—slow unloading” (SU)

Figure 8 presents the relationships between the hydrostatic pressure and the sample volume change and temperature inside the high-pressure cell for various compression rates and for a decompression rate of 0.5 MPa/s.

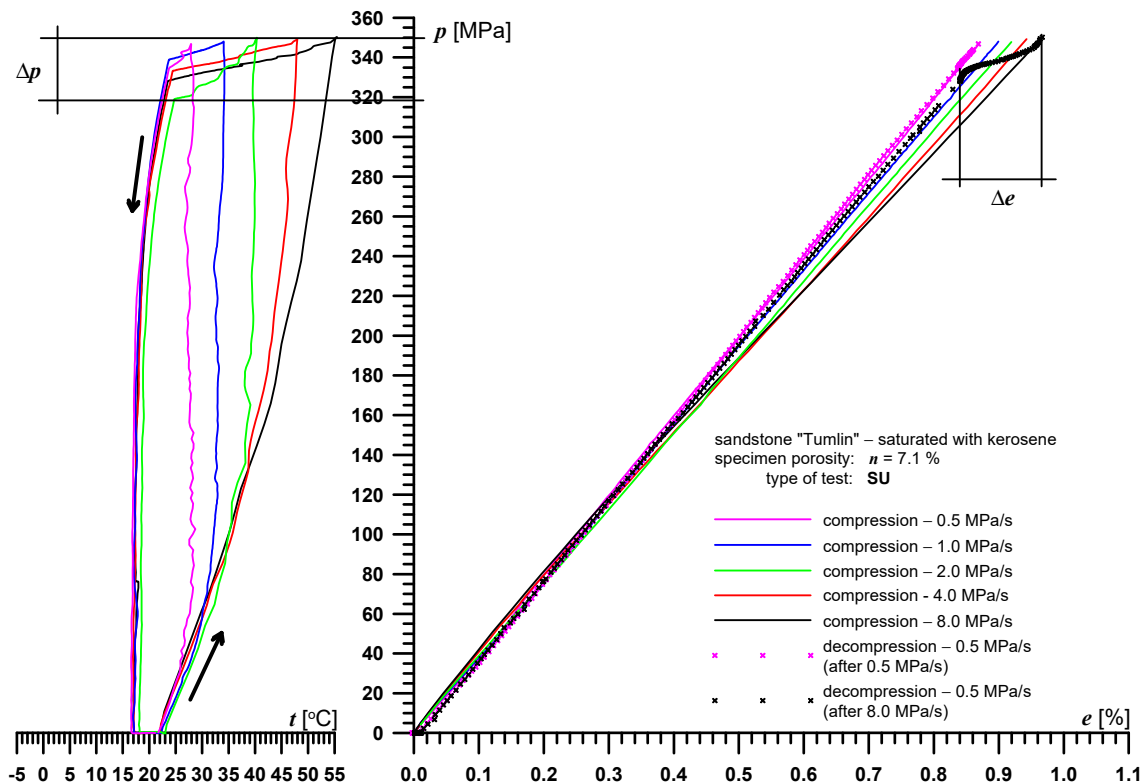


Figure 8. SU test result for Tumlin sandstone. **Left:** relationship between hydrostatic pressure and temperature (the arrows indicate the direction of change of hydrostatic pressure), **right:** relationship between hydrostatic pressure and volume change.

It is clear that the higher was the compression rate, the larger were the corresponding increases in liquid temperature inside the cell. It should also be expected that the pressure drops Δp accompanying temperature stabilization will increase with increasing compression rate. Both these relationships were generally confirmed by the experimental results, as shown in Figure 8.

The compression lines presented in Figure 8 are quite surprising. It is usual to find that the deformability of a sample decreases with increasing loading rates. The compression lines in Figure 8, however, show that the higher the compression rate, the higher the deformability of the sample. Filtration is again the process most likely responsible for this behavior. We again have a situation in which the increase in pore pressure is delayed relative to the pressure increase inside the cell, where the higher the compression rate, the larger the difference between the pressures. As a consequence, the higher the compression rate, the higher the sample deformability, as is illustrated very well by the values of volumetric moduli of compressibility $K_{s(c)}$ shown in Table 2.

Table 2. Volumetric moduli of compressibility for compression ($K_{s(c)}$) and decompression ($K_{s(d)}$); SU test, Tumlin sandstone.

Rock Compressibility Modulus (K_s)	Compression Rate					Decompression Rate
$K_{s(c)}$	8.0 MPa/s	4.0 MPa/s	2.0 MPa/s	1.0 MPa/s	0.5 MPa/s	0.5 MPa/s
$K_{s(d)}$	34.6 GPa	36.6 GPa	37.9 GPa	38.4 GPa	40.1 GPa	40.0 GPa

The course of the decompression line (always for the same rate of 0.5 MPa/s) was slightly different for various compression rates, but in the final unloading phase it always overlapped with the line labelled “decompression—0.5 MPa/s⁻¹” in Figure 8. Thus, two de-

compression lines are shown in Figure 8: the first—starting after the slowest compression—labelled “decompression— 0.5 MPa/s^{-1} (after 0.5 MPa/s^{-1})” and the second—starting after the fastest decomposition—labelled “decompression— 0.5 MPa/s^{-1} (after 8.0 MPa/s^{-1})”. It can be seen that the second decomposition line approaches the first line as the load decreases, eventually overlapping at pressure values of $p \leq 140 \text{ MPa}$. The volumetric modulus of compressibility $K_{s(d)}$ calculated for the line “decompression— 0.5 MPa/s^{-1} (after 0.5 MPa/s^{-1})” has the value 40.0 GPa (cf. Table 2) and is virtually identical to the volumetric modulus of compressibility for compression $K_{s(c)}$ performed at a loading rate of 0.5 MPa/s .

(D) “Various loading—fast unloading” (FU)

The test results are presented in Figure 9. In this test, various compression rates were combined with a single decomposition rate, with the value 8.0 MPa/s . The figure does not include any results for the lowest loading rate of 0.5 MPa/s . This is because of a malfunction of the device during the experiment.

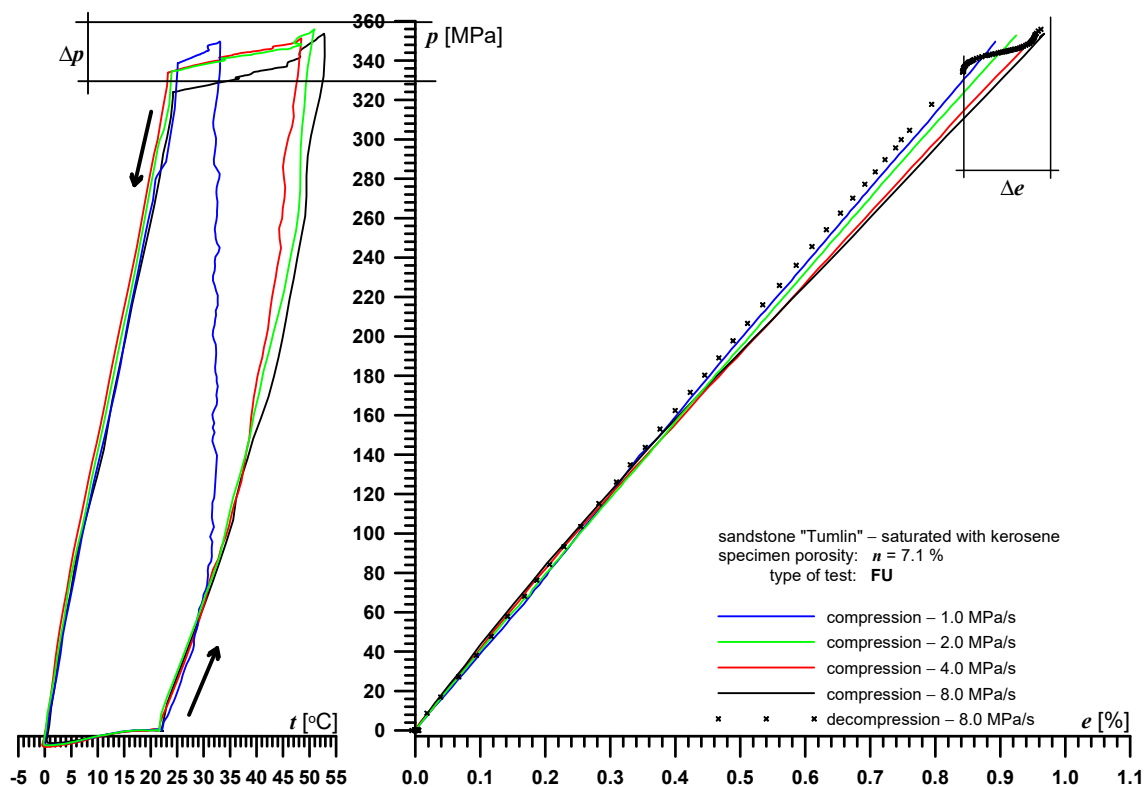


Figure 9. FU test result for Tumlin sandstone. **Left:** relationship between hydrostatic pressure and temperature (the arrows indicate the direction of change of hydrostatic pressure), **right:** relationship between hydrostatic pressure and volume change.

The differences between the $p(t)$ relationships presented in Figures 8 and 9 should be considered purely quantitative. The higher decomposition rate merely resulted in a larger temperature drop (Figures 8 and 9, left). In the case of the $p(e)$ curves for the FU test (Figure 9, right) it may be concluded that the compressibility curve obtained for compression and decomposition performed at the same rate of 8.0 MPa/s is an envelope containing all the other curves. Table 3 provides a list, similar to that for the SU test, of the moduli of compressibility calculated for the individual compressibility curves shown in Figure 8. The values of the moduli in Table 3 are not significantly different from the corresponding values in Table 2, and the previously observed increase in sample deformability related to the increased compression rate was also confirmed in this case. There appears to be no doubt that this phenomenon is related to filtration.

Table 3. Volumetric moduli of compressibility for compression ($K_{s(c)}$) and decompression ($K_{s(d)}$); FU test, Tumlin sandstone.

Rock Compressibility Modulus (K_s)	Compression Rate					Decompression Rate
	8.0 MPa/s	4.0 MPa/s	2.0 MPa/s	1.0 MPa/s	0.5 MPa/s	
$K_{s(c)}$	34.9 GPa	35.7 GPa	37.4 GPa	38.4 GPa	undetermined	0.5 MPa/s
$K_{s(d)}$						39.2 GPa

8. Summary

The experimental results presented and discussed above prove that the rate of change of the confining pressure significantly impacts the result of the drained compressibility test of “ $p_p = p$ ” type. The respective values of the K_s moduli and of the α coefficients are given in Tables 4 and 5, and their dependence on compression rates is shown in Figures 10 and 11.

Table 4. Volumetric moduli of compressibility and Biot’s coefficients for compression ($K_{s(c)}$, $\alpha_{(c)}$) and decompression ($K_{s(d)}$, $\alpha_{(d)}$); SU test, Tumlin sandstone.

Rock Compressibility Modulus (K_s , K) Biot Coefficient (α)	Compression Rate					Decompression Rate
	8.0 MPa/s	4.0 MPa/s	2.0 MPa/s	1.0 MPa/s	0.5 MPa/s	
$K_{s(c)}$	34.6 GPa	36.6 GPa	37.9 GPa	38.4 GPa	40.1 GPa	0.5 MPa/s
$K_{s(d)}$						40.0 GPa
K				21.5 GPa		
$\alpha_{(c)}$	0.38	0.41	0.43	0.44	0.46	
$\alpha_{(d)}$						0.46

Table 5. Volumetric moduli of compressibility and Biot’s coefficients for compression ($K_{s(c)}$, $\alpha_{(c)}$) and decompression ($K_{s(d)}$, $\alpha_{(d)}$); FU test, Tumlin sandstone.

Rock Compressibility Modulus (K_s , K) Biot Coefficient (α)	Compression Rate					Decompression Rate
	8.0 MPa/s	4.0 MPa/s	2.0 MPa/s	1.0 MPa/s	0.5 MPa/s	
$K_{s(c)}$	34.9 GPa	35.7 GPa	37.4 GPa	38.4 GPa	undetermined	0.5 MPa/s
$K_{s(d)}$						39.2 GPa
K				21.5 GPa		
$\alpha_{(c)}$	0.38	0.40	0.43	0.44	undetermined	
$\alpha_{(d)}$						0.45

It can be seen, in particular, that the deformability of the studied rock increases with increasing compression rates, manifested in a decreased value of the volumetric modulus of compressibility of the rock skeleton K_s . The cause of this phenomenon seems to be the process of fluid filtration into the studied sample. This process causes the equilibration of hydrostatic and pore pressures to be extended over a longer time, and thus, the main condition for correct determination of the modulus of compressibility of the rock skeleton K_s , namely that the pore pressure is equal to the hydrostatic pressure, may no longer be satisfied. It may be concluded, on the other hand, that filtration serves as a “shock absorber”, preventing excessively sudden rock deformations during fast loading (The author is fully aware that this statement is not particularly original. This is, after all, how a shock absorber works in a car suspension system.)

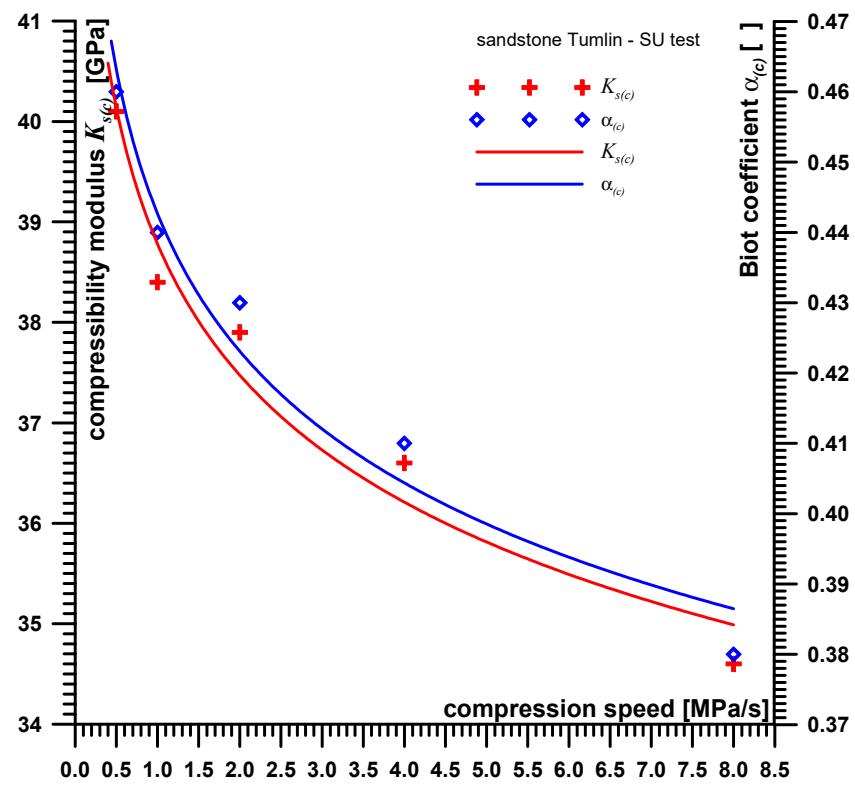


Figure 10. Relationship between the values of the α coefficient and K_s modulus and the compression rate—SU test; Tumlin sandstone.

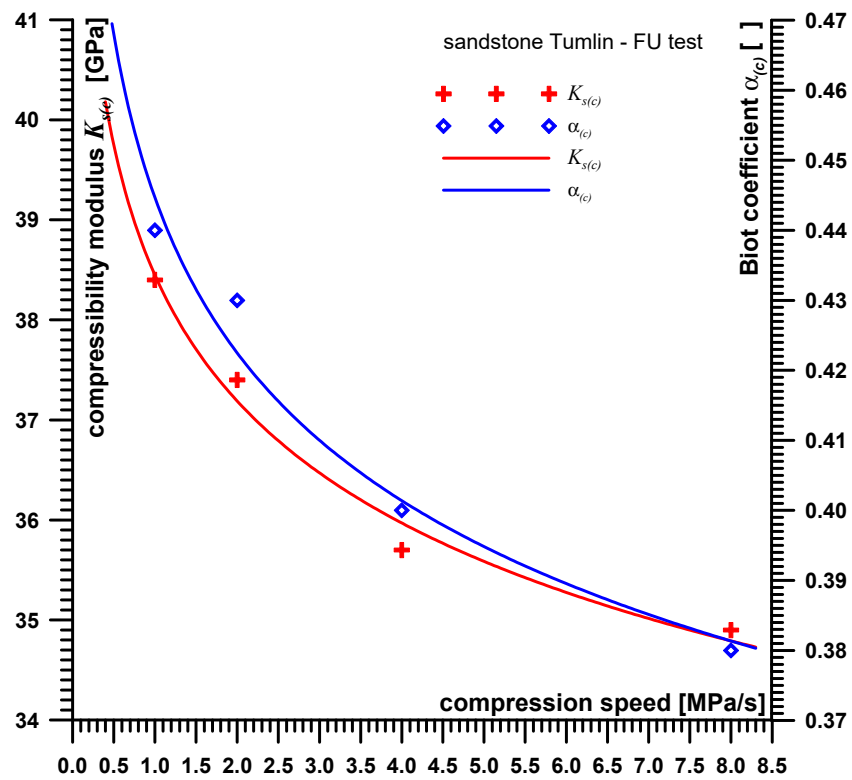


Figure 11. Relationship between the values of the α coefficient and K_s modulus and the compression rate—FU test; Tumlin sandstone.

Looking at the relationship between the compression rate and the value of Biot's coefficient, we see that it is inversely proportional: the faster the rock is loaded, the smaller is the value of α . This effect should be considered in the context of the form of Equation (6). In this equation, Biot's coefficient is a weight determining the role of the pore fluid in shaping the stress state inside the rock. The results obtained indicate that this role is less significant when rock loading is faster.

9. Conclusions

The results of the laboratory tests shown above should be treated as a warning against the indiscriminate application of the equations of the poroelastic Biot medium to model the phenomena occurring in the fluid-filled rock mass. When creating his model, Maurice Anthony Biot assumed (cf. [5]) that the pore pressure p_p in the pore space of the medium should meet the condition $p_p = \text{const}$. The research results presented in this paper demonstrate what happens if this condition is not met. In particular, it follows from them that some material constants cease to be constant and, in addition, they become functions of the pore pressure rate, and thus indirectly functions of time, which completely changes the nature of Equations (1) and (2).

Finally, it should also be noted that this work did not analyze the influence of the value of a significant structural material constant, namely porosity (n), on the results of the discussed compressibility experiments. For the studied Tumlin sandstone, $n \leq 8\%$, which means that the pore volume required to be filled with liquid was relatively small. It, thus, seems justified to assume that in the case of a rock with significantly higher porosity (e.g., 20%), the influence of changes in the rate of compression or decompression on the final result will be qualitatively identical, but quantitatively much greater.

Funding: This work was performed in 2019, as a part of statutory works executed at Strata Mechanics Research Institute of the Polish Academy of Sciences in Kraków, funded by the Ministry of Science and Higher Education.

Institutional Review Board Statement: Not applicable.

Informed Consent Statement: Not applicable.

Data Availability Statement: The study did not report any data.

Conflicts of Interest: The author declare no conflict of interest.

References

1. EUROSTAT. Available online: <https://ec.europa.eu/eurostat/databrowser/view/ten00122/default/table?lang=en> (accessed on 10 February 2021).
2. Tajduś, K.; Sroka, A.; Misa, R.; Tajduś, A.; Meyer, S. Surface deformations caused by the convergence of large underground gas storage facilities. *Energies* **2020**, *14*, 402. [\[CrossRef\]](#)
3. Liu, J.; Hunfeld, L.B.; Niemeijer, A.R.; Spiers, J.C. Frictional properties of simulated shale-coal fault gouges: Implications for induced seismicity in source rocks below Europe's largest gas field. *Int. J. Coal Geol.* **2020**, *226*. [\[CrossRef\]](#)
4. Hunfeld, L.B.; Niemeijer, A.R.; Spiers, J.C. Frictional properties of simulated fault gouges from the seismogenic Groningen gas field under in situ P-T chemical conditions. *J. Geophys. Res. Solid Earth* **2017**, *122*, 8969–8989. [\[CrossRef\]](#)
5. Biot, M.A. General Theory of Three-Dimensional Consolidation. *J. Appl. Phys.* **1941**, *12*, 155–164. [\[CrossRef\]](#)
6. Nur, A.; Byerlee, J.D. An Exact Effective Stress Law for Elastic Deformation of Rock with Fluids. *J. Geophys. Res.* **1971**, *76*, 6414–6419. [\[CrossRef\]](#)
7. Walsh, J.B. The effect of cracks on compressibility of rock. *J. Geophys. Res.* **1965**, *70*, 381–389. [\[CrossRef\]](#)
8. Fabre, D.; Gustkiewicz, J. Influence of rock porosity on the Biot's coefficient. In *Poromechanics—A Tribute to Maurice A. Biot. Proceedings of the Biot Conference on Poromech., Louvain-la-Neuve, Belgium, 14–16 September 1998*; Thismus, J.-F., Abousleiman, Y., Cheng, A.H.-D., Coussy, O., Detournay, E., Eds.; Balkema: Rotterdam, The Netherlands, 1998; pp. 561–566.
9. Gustkiewicz, J. Compressibility of rocks with a special consideration given to pore pressure. In *Poromechanics—A Tribute to Maurice A. Biot. Proceedings of the Biot Conference on Poromech., Louvain-la-Neuve, Belgium, 14–16 September 1998*; Thismus, J.-F., Abousleiman, Y., Cheng, A.H.-D., Coussy, O., Detournay, E., Eds.; Balkema: Rotterdam, The Netherlands, 1998; pp. 573–577.
10. Gustkiewicz, J. Volumetric deformations of a rock and its pores. *Arch. Min. Sci.* **1989**, *34*, 593–609. (In Polish)
11. Biot, M.A. Theory of elasticity and consolidation for a porous anisotropic solid. *J. Appl. Phys.* **1955**, *26*, 182–185. [\[CrossRef\]](#)
12. Biot, M.A.; Willis, D.G. The Elastic Coefficients of the Theory of Consolidation. *J. Appl. Mech.* **1957**, *24*, 594–601.

13. Carroll, M.M. An Effective Stress Law for Anisotropic Elastic Deformation. *J. Geophys. Res.* **1979**, *84*, 7510–7512. [[CrossRef](#)]
14. Cheng, A.H.-D.; Abousleiman, Y.; Roegiers, J.-C. Review of Some Poroelastic Effects in Rock Mechanics. *Int. J. Rock Mech. Min. Sci. Geomech. Abstr.* **1993**, *30*, 1119–1126. [[CrossRef](#)]
15. Roegiers, J.-C.; Cui, L.; Bai, M. Poroelasticity applications. In *Mechanics of Jointed and Faulted Rocks, Proceedings of the 3rd Int. Conference Mech. Joint. & Fault. Rock—MJFR-3, Vienna, Austria, 6–9 April 1998*; Rossmannith, H.-P., Ed.; Balkema: Rotterdam, The Netherlands, 1998; pp. 39–48.
16. Boutéca, M.; Guéguen, Y. Mechanical Properties of Rocks: Pore Pressure and Scale Effects. *Oil Gas Sci. Technol. Rev. IFP* **1999**, *54*, 703–714.
17. Cowin, S.C.; Benalla, M. Graphical Illustrations for the Nur-Byerlee-Carroll Proof of the Formula for the Biot Effective Stress Coefficient in Poroelasticity. *J. Elast.* **2011**, *104*, 133–141. [[CrossRef](#)]
18. Ahmed, S.; Müller, T.M.; Madadi, M.; Calo, V. Drained pore modulus and Biot coefficient from pore-scale digital rock simulations. *Int. J. Rock Mech. Min. Sci.* **2019**, *114*, 62–70. [[CrossRef](#)]
19. Paterson, M.S.; Wong, T.-f. *Experimental Rock Deformation—The Brittle Field*, 2nd ed.; Springer: Berlin/Heidelberg, Germany, 2005.
20. Jaeger, J.C.; Cook, N.G.W.; Zimmerman, R.W. *Fundamentals of Rock Mechanics*, 4th ed.; Blackwell Publishing: Malden, MA, USA; Oxford, UK; Carlton, Australia, 2007.
21. Wang, H.F. *Theory of Linear Poroelasticity with Applications to Geomechanics and Hydrogeology*, 1st ed.; Princeton University Press: Princeton, NJ, USA; Oxford, UK, 2000.
22. Vasquez, G.F.; Junior, E.A.V.; Ribeiro, C.J.B.; Leão, M.; Justen, J.C.R. Experimental determination of the effective pressure coefficients for Brazilian limestones and sandstones. *Revista Brasileira Geofísica* **2009**, *27*, 43–53. [[CrossRef](#)]
23. Salemi, H.; Inglauer, S.; Rezagholilou, A.; Sarmadivaleh, M. Laboratory measurement of Biot’s coefficient and pore pressure influence on poroelastic rock behaviour. *APPEA J.* **2018**, *58*, 182–189. [[CrossRef](#)]
24. He, J.; Rui, Z.; Ling, K. A new method to determine Biot’s coefficients of Bakken samples. *J. Nat. Gas Sci. Eng.* **2016**, *35 Pt A*, 259–264. [[CrossRef](#)]
25. Makhnenko, R.Y.; Labuz, J.F. Saturation of Porous Rock and Measurement of the B coefficient. In *Proceedings of the 47th US Rock Mechanics/Geomechanics Symposium 2013, San Francisco, CA, USA, 23–26 June 2013*; ARMA: San Francisco, CA, USA, 2013.
26. Nermoen, A.; Korsnes, R.; Christensen, H.F.; Trads, N.; Hiorth, A.; Madland, M.V. Measuring the Biot Stress Coefficient and its Implications of on the Effective Stress Estimate. In *Proceedings of the 47th US Rock Mechanics/Geomechanics Symposium 2013, San Francisco, CA, USA, 23–26 June 2013*; ARMA: San Francisco, CA, USA, 2013.
27. Ingraham, M.D.; Bauer, S.J.; Issen, K.A.; Dewers, T.A. Evolution of permeability and Biot coefficient at high mean stresses in high porosity sandstone. *Int. J. Rock Mech. Min. Sci.* **2017**, *96*, 1–10. [[CrossRef](#)]
28. Lion, M.; Skoczylas, F.; Ledésert, B. Determination of the main hydraulic and poro-elastic properties of a limestone from Bourgogne, France. *Int. J. Rock Mech. Min. Sci.* **2004**, *41*, 915–925. [[CrossRef](#)]
29. Yuan, H.; Agostini, F.; Duan, Z.; Skoczylas, F.; Talandier, J. Measurement of Biot’s coefficient for CO_x argillite using gas pressure technique. *Int. J. Rock Mech. Min. Sci.* **2017**, *92*, 72–80. [[CrossRef](#)]
30. Rychlewski, J. Note on the beginning of plastic deformation in a body under uniform pressure. *Archives Mécanique Appliquée* **1965**, *17*, 405–412.
31. Nowakowski, A.; Nurkowski, J. About some problems related to determination of the e.g. Biot coefficient for rocks. *Arch. Min. Sci.* **2021**, *66*, 133–150.
32. Kovári, K.; Tisa, A.; Einstein, H.H.; Franklin, J.A. Suggested Methods for Determining the Strength of Rock Materials in Triaxial Compression: Revised Version. *Int. J. Rock Mech. Min. Sci. Geomech. Abstr.* **1983**, *20*, 283–290.
33. Długosz, M.; Gustkiewicz, J.; Wysocki, A. Apparatus for investigation of rock in triaxial state of stress. Part I. Characteristics of the apparatus and of the investigation method. *Arch. Min. Sci.* **1981**, *26*, 17–28.
34. Długosz, M.; Gustkiewicz, J.; Wysocki, A. Apparatus for investigation of rock in triaxial state of stress. Part II. Some investigation results concerning certain rocks. *Arch. Min. Sci.* **1981**, *26*, 29–41.
35. Nurkowski, J. An inductive strain sensor for operation in high pressure environments. *Int. J. Rock Mech. Min. Sci. Geomech. Abstr.* **2004**, *41*, 175–180. [[CrossRef](#)]
36. Nowakowski, A.; Młynarczyk, M.; Ratajczak, T.; Gustkiewicz, J. *Wpływ Warunków Termicznych na Zmianę Niektórych Właściwości Fizycznych i Strukturalnych Wybranych Skał (Influence of Thermal Conditions on Changes of Some Physical and Structural Properties of Selected Rocks)*; Transactions of the Strata Mechanics Research Institute: Kraków, Poland, 2003; Volume 5. (In Polish)
37. Nurkowski, J. Wykorzystanie półprzewodnikowych przetworników do pomiaru temperatury w warunkach wysokiego ciśnienia (Use of semiconductor transducers for temperature measurement in high pressure conditions). In *Proceedings of XXXV Intercollegiate Conference of Metrologists MKM’95, Zielona Góra, Poland, 21–23 September 1995*; University of Engineering in Zielona Góra: Zielona Góra, Poland, 1995; Volume 1, pp. 300–303. (In Polish)